ChemComm

COMMUNICATION

View Article Online
View Journal | View Issue

Cite this: *Chem. Commun.*, 2014, **50**, 292

Received 13th August 2013,
Accepted 28th October 2013

DOI: 10.1039/c3cc46180g

www.rsc.org/chemcomm

Investigations on the crystal plane effect of ceria on gold catalysis in the oxidative dehydrogenation of alcohols and amines in the liquid phase†

Min Wang, Feng Wang,* Jiping Ma, Mingrun Li, Zhe Zhang, Yehong Wang, Xiaochen Zhang and Jie Xu*

Gold nanoparticles supported on ceria{110} crystal planes were more reactive than on ceria{111} and {100} in the oxidative dehydrogenation of alcohols. Kinetic analysis and a Hammett plot suggest that hydride transfer is involved, and the cationic gold is catalytically active.

Catalytic effects of ceria crystal planes have been examined for gas-phase reactions of small molecules, such as CO_x, H_2O, H_2, CH_4 and NO_x.[1] Flytzani-Stephanopoulos *et al.* showed that the ceria nanorod enclosed by {110} and {100} planes was most active for gold stabilization/activation in the water-gas shift reaction (WGS).[1d] Shen *et al.* showed that gold nanoparticles anchored onto the {111} plane of ceria were highly active for CO oxidation.[1e] Different crystal planes have remarkably different functions in catalysis.[2] On the other hand, ceria based catalysts have also catalyzed organic transformations, such as hydration and dehydration, alkylation, ketonization and redox reactions.[3] Our recent study showed that ceria could catalyze C–C coupling and C–O cleavage reactions.[4] These reactions involving large molecules in the liquid phase are much more complex than those in the gas phase, but usually the reactions were correlated with the acid–base properties of ceria, and the crystal plane effect is greatly neglected.[5]

Oxidation of alcohols and amines is a convenient and direct synthesis way for carbonyl compounds, imines and amines.[6] Corma *et al.* described the size effect of ceria on the alcohol oxidation.[7] Some others focused on metal phases,[8] ceria composition and structure,[9] magnetic recycle[10] and preparation methods.[11] Few studies are known for Au–ceria composite nanomaterial with respect to the relationship of structure (crystal planes of ceria on gold)–activity.

Herein we report the Au/ceria catalyst for the conversion of alcohols to aldehydes or ketones, and amines to imines *via* oxidative dehydrogenation. Both types of reaction achieve moderate to excellent yields. Importantly, the present study reveals that the active plane for C–H and N–H bond activation is the {110} plane on nanorod ceria. Characterization by Raman and X-ray photoelectron spectroscopy (XPS) shows that positively charged gold dominates in nanorod Au/ceria possibly *via* the interaction with oxygen vacancy sites. Furthermore, kinetic analysis and the Hammett plot suggest that hydride transfer is involved in C–H bond activation, and the cationic gold is catalytically active.

CeO_2 nanorods (CeO_2–R), nanocubes (CeO_2–C), and nanooctahedra (CeO_2–O) were prepared according to the literature.[12] The sizes of the CeO_2–R, CeO_2–C, and CeO_2–O were (10 × 20–110) nm, 10–50 nm, and 50–135 nm with the surface area of 80 $m^2\ g^{-1}$, 33 $m^2\ g^{-1}$ and 22 $m^2\ g^{-1}$, respectively. Approx. 9 nm CeO_2 nanoparticles (CeO_2–P) were synthesized for comparison. Gold nanoparticles were deposited on ceria by a deposition–precipitation method.[1d] The as-synthesized ceria is face-centered cubic (fcc, space group: $Fm\bar{3}m$) (Fig. S1, ESI†). The TEM images (Fig. S2, ESI†) indicate that the shape of ceria remains unchanged before and after gold deposition. Similar to the literature,[1a,b] HRTEM observations confirm that CeO_2–R exposes 51% {110} and 49% {100} planes. Thus, the corresponding {110} and {100} surface area in CeO_2–R is calculated to be 41 $m^2\ g^{-1}$ and 39 $m^2\ g^{-1}$, respectively. Nearly 100% of CeO_2–C is enclosed with {100}, and CeO_2–O with {111} planes (Fig. 1). The enclosed planes are confirmed by the average lattice distances for {110}, {100} and {111} planes, which are 0.19 nm, 0.27 nm and 0.32 nm, respectively. HRTEM images also indicate that gold nanoparticles with the diameter of 4–5 nm are located on the CeO_2–R{110}, CeO_2–C{100} and CeO_2–O{111} planes.

The Au/CeO_2 catalysts were initially evaluated in the oxidation of benzyl alcohol to benzaldehyde. Ceria alone is inactive (Table 1, entry 1). The size of gold among all catalysts is nearly identical, as evidenced by HRTEM. All catalysts offered >99% selectivity for benzaldehyde. Au/CeO_2–C, Au/CeO_2–O and Au/CeO_2–P gave low to moderate conversion of 5%, 42%, and 79%, respectively (Table 1, entries 2–4). Remarkably the conversion reached 96% when Au/CeO_2–R was used (Table 1, entry 5). This could exclude the support size effect because CeO_2–P is much smaller than CeO_2–R. The reaction ceased at 8% in an Ar atmosphere (Table 1, entry 6), and proceeded comparably well in 1 atm of air (Table 1, entry 7) or oxygen, indicating that oxygen is indispensable and its mass transfer

Dalian National Laboratory for Clean Energy, State Key Laboratory of Catalysis, Dalian Institute of Chemical Physics, Chinese Academy of Sciences, Dalian, 116023, P. R. China. E-mail: wangfeng@dicp.ac.cn, xujie@dicp.ac.cn; Web: www.fwang.dicp.ac.cn

† Electronic supplementary information (ESI) available: The experimental and characterization data. See DOI: 10.1039/c3cc46180g

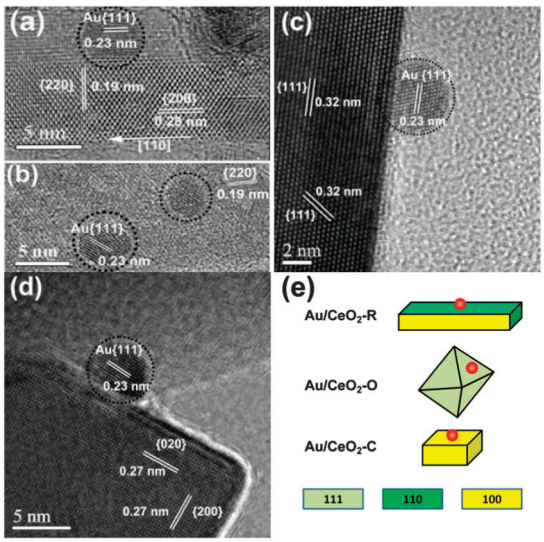

Fig. 1 High-resolution TEM (HRTEM) images of the Au/ceria catalysts. Side view (a) and top view (b) of Au/CeO_2–R, (c) Au/CeO_2–O, (d) Au/CeO_2–C, (e) schemes of nanostructured ceria with different crystal plane enclosures and the supporting for gold.

Table 1 Oxidation of benzyl alcohol over various Au/CeO_2 catalysts[a]

Entry	Catalyst	Conversion [%]	Selectivity [%]
1[b]	CeO_2–R	3	>99
2	Au/CeO_2–C	5	>99
3	Au/CeO_2–O	42	>99
4	Au/CeO_2–P	79	>99
5	Au/CeO_2–R	96	>99
6[c]	Au/CeO_2–R	8	>99
7[d]	Au/CeO_2–R	94	>99
8[e]	Au/CeO_2–R	20	>99

[a] Reaction conditions: 1 mmol benzyl alcohol, 5 mL chlorobenzene, 2 equiv. Cs_2CO_3, catalyst (0.1 mol% Au), 90 °C, 8 h. [b] 0.02 g. [c] In 1 atm Ar. [d] Air was used instead of pure oxygen. [e] Without Cs_2CO_3.

is not limited. Base additives, such as Cs_2CO_3, are necessary for the reaction (Table 1, entry 8).

We further found that Au/CeO_2–R could catalyze the oxidation of other primary or secondary alcohols with moderate to high yields of aldehydes or ketones (Table 2). The reactions are very selective regardless of the presence of electron-donating or electron-withdrawing substituents (Table 2, entries 1–7). The olefinic C=C double bond is not affected (Table 2, entry 8). Secondary aromatic alcohols with electron-donating or electron-withdrawing groups are smoothly converted to the corresponding ketones (Table 2, entries 9–12). Furfuryl alcohol and aliphatic alcohols are reluctant to react (Table 2, entries 13–15). Au/CeO_2–R was filtered out, washed, and reused for three cycles with comparable activities (1st reuse: 99%, 2nd 98%, 3rd 98%, Fig. S3, ESI†). No further conversion of benzyl alcohol was observed after filtering out the catalyst during reaction (hot filtration) (Fig. S4, ESI†). The inductively coupled plasma-mass analysis revealed that no Au species were detected in the reaction mixture, indicating that Au is well stabilized on ceria.

Catalytic results motivated us to conduct more deep investigations on Au–ceria structure. We hypothesized that gold might adsorb on oxygen vacancy sites ($V_O^{\bullet\bullet}$). The change in $V_O^{\bullet\bullet}$ content

Table 2 Oxidation of alcohols over the Au/CeO_2–R catalyst[a]

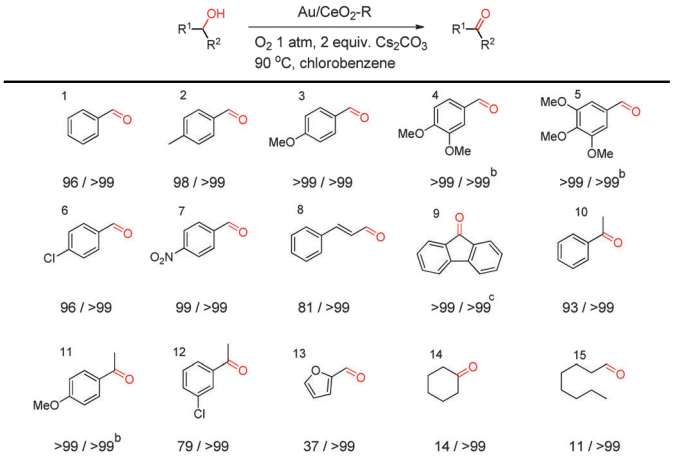

[a] Reaction conditions: 1 mmol alcohol, 5 mL chlorobenzene, catalyst (0.1 mol% Au), 2 equiv. Cs_2CO_3, 1 atm O_2; 90 °C, 8 h. The results are represented as conversion/selectivity. [b] 4 h. [c] 2 h.

after gold deposition could reflect this interaction. Raman spectroscopy with the 514 nm laser line only explores surface layer information and thus is used for this purpose. All ceria exhibit F_{2g} vibrational modes of the fluorite phase at 462 cm^{-1} (Fig. S5, ESI†). Weak bands at 595 cm^{-1} are ascribed to the Frenkel-type oxygen defects.[13] After gold deposition, the peak at 462 cm^{-1} red-shifted to 446, 450, and 450 cm^{-1} for Au/CeO_2–R, Au/CeO_2–O and Au/CeO_2–C, respectively. This is possibly caused by surface distortion because of the gold–ceria interaction. The more the red-shift is, the stronger the gold–ceria interaction is. Because ceria–R is largely enclosed by {110} planes, we may postulate that the gold–ceria interaction on {110} planes is stronger than that on other crystal phases. Furthermore, the ratio of the integrated peak areas of 595 and 462 cm^{-1} (A595/A462) can be an indicator for quantifying the relative surface concentration of $V_O^{\bullet\bullet}$ sites.[14] Theoretical calculations have shown that the formation energy of $V_O^{\bullet\bullet}$ follows the sequence of {110} < {100} < {111}.[15] CeO_2 nanorods possess the highest content of $V_O^{\bullet\bullet}$ followed by nanocubes and nanooctahedra, which well agrees with the calculation results (Fig. S6, ESI†). In comparison with the ceria support, the $V_O^{\bullet\bullet}$ sites almost completely disappeared for Au/CeO_2–R, but were still detectable for Au/CeO_2–O and Au/CeO_2–C. The loss sequence of $V_O^{\bullet\bullet}$ could also indicate the sequence of the strength of the gold–ceria interaction with crystal planes of {110} > {111} > {100}. It is reported that the ceria{111} surface is O-terminated, and the polar {100} surface is either Ce-terminated or O-terminated with no more than 50% surface oxygen coverage due to relaxation.[16] In either case, nevertheless, the $V_O^{\bullet\bullet}$ on the {100} surface may mainly locate on the subsurface which weakens the interaction with gold. This accounts for minor loss of $V_O^{\bullet\bullet}$ for CeO_2 nanocubes compared to CeO_2 nanooctahedra. The gold$-V_O^{\bullet\bullet}$ interaction may stabilize the positively charged gold as analyzed by XPS (Fig. S7 and Table S1, ESI†). Positively charged gold dominates in Au/CeO_2–R with content of 71%, followed by Au/CeO_2–O and Au/CeO_2–C.

Correlating $-\ln(1 - C)$ (C stands for conversion) against reaction time (ks) indicates a linear relationship and a first order reaction with respect to benzyl alcohol (Fig. S8a, ESI†). Previous studies showed that the C–H bond cleavage was the rate-determining

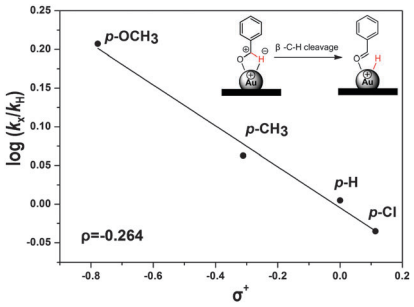

Fig. 2 Hammett plot for the oxidation of substituted benzyl alcohols catalyzed by Au/CeO_2–R. The inset is the proposed way for the cleavage of the C–H bond by cationic gold.

step in the oxidation of alcohols over noble metal catalysts.[17] The apparent activation energy, E_a, associated with the C–H bond cleavage is determined from the Arrhenius plot (Fig. S8b and S9, ESI†). The least-square fit analysis yields an E_a value of 24.5 kJ mol^{-1} for Au/CeO_2–R, which is lower than 35.1 kJ mol^{-1} for Au/CeO_2–P and 42.3 kJ mol^{-1} for Au/CeO_2–O. And, it is also lower than the reported values of 28.1 kJ mol^{-1},[17a] 32.3 kJ mol^{-1},[18] 45.7 kJ mol^{-1} (ref. 19) and 45.8 kJ mol^{-1}.[20] This result indicates that the ceria{110}-supported positively charged gold can greatly lower the C–H bond activation energy, and thus increase catalytic activity. The reaction rate increased with increasing cationic gold content (Fig. S10, ESI†).

A linear relationship between $\log(k_X/k_H)$ and Brown–Okamoto constant σ^+ (Fig. 2) was established for the oxidation of substituted benzyl alcohols (X = *p*-Cl, *p*-H, *p*-Me and *p*-OMe). The resulting Hammett parameter ρ was −0.264, suggesting that the reaction is substituent-sensitive and carbocation intermediates are involved. Electron-donating groups can stabilize the carbocation intermediates and thus are more favored to be oxidized.[17b] Based on our previous study, we postulate that the positively charged gold may favor the hydride abstraction *via* β-H elimination to form gold hydride, generating a carbocation-type intermediate.

Besides alcohol oxidation, amines oxidation could also smoothly take place over Au/CeO_2–R. This extends its application to the conversion of benzylamine in the presence of electron-donating or electron-withdrawing substituents and heterocycle amines to *N*-benzylidene-methanamine derivatives with moderate to high activity and selectivity (Table 3). The TOF for the oxidation of benzylamine was 93.9 h^{-1},[21] which is higher than other gold catalysts of Au$(OAc)_3$/CeO_2 (3.2 h^{-1}),[6d] Au/Al_2O_3 (0.3 h^{-1}) and Au powder (0.001 h^{-1}).[6e]

Table 3 Oxidation of amines over the Au/CeO_2–R catalyst[a]

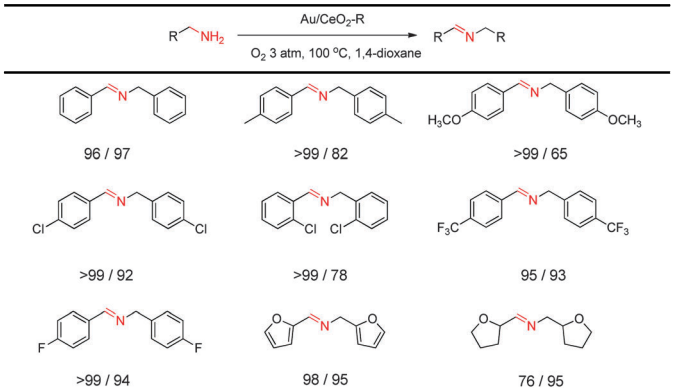

[a] Reaction conditions: 0.2 mmol substrate, catalyst (0.25 mol% Au), 2 mL 1,4-dioxane, 3 atm oxygen, 100 °C, 6 h. The results were presented as conversion/selectivity. The main byproducts were aldehydes and nitriles.

In summary, we have demonstrated that gold nanoparticles supported on the ceria{110} crystal planes were more reactive than on the {111} and {100} crystal planes in the oxidative dehydrogenation of alcohols and amines.

This work was supported by the National Natural Science Foundation of China (21303183, 21273231, 21233008) and Hundred Person Project of the Chinese Academy of Sciences.

Notes and references

1 (*a*) J. L. He, T. Xu, Z. H. Wang, Q. H. Zhang, W. P. Deng and Y. Wang, *Angew. Chem., Int. Ed.*, 2012, **51**, 2438; (*b*) N. Ta, J. Y. Liu and W. J. Shen, *Chin. J. Catal.*, 2013, **34**, 838; (*c*) X. S. Huang, H. Sun, L. C. Wang, Y. M. Liu, K. N. Fan and Y. Cao, *Appl. Catal., B*, 2009, **90**, 224; (*d*) R. Si and M. Flytzani-Stephanopoulos, *Angew. Chem., Int. Ed.*, 2008, **47**, 2884; (*e*) N. Ta, J. Y. Liu, S. Chenna, P. A. Crozier, Y. Li, A. L. Chen and W. J. Shen, *J. Am. Chem. Soc.*, 2012, **134**, 20585.
2 X. W. Xie, Y. Li, Z. Q. Liu, M. Haruta and W. J. Shen, *Nature*, 2009, **458**, 746.
3 (*a*) M. Tamura, A. Satsuma and K.-i. Shimizu, *Catal. Sci. Technol.*, 2013, **3**, 1386; (*b*) Y. Zhang, F. Hou and Y. W. Tan, *Chem. Commun.*, 2012, **48**, 2391; (*c*) L. Vivier and D. Duprez, *ChemSusChem*, 2010, **3**, 654.
4 Y. H. Wang, F. Wang, Q. Song, Q. Xin, S. T. Xu and J. Xu, *J. Am. Chem. Soc.*, 2013, **135**, 1506.
5 K. Deori, D. Gupta, B. Saha, S. K. Awasthi and S. Deka, *J. Mater. Chem. A*, 2013, **1**, 7091.
6 (*a*) M. T. Schumperli, C. Hammond and I. Hermans, *ACS Catal.*, 2012, **2**, 1108; (*b*) B. N. Wigington, M. L. Drummond, T. R. Cundari, D. L. Thorn, S. K. Hanson and S. L. Scott, *Chem.–Eur. J.*, 2012, **18**, 14981; (*c*) Q. H. Zhang, W. P. Deng and Y. Wang, *Chem. Commun.*, 2011, **47**, 9275; (*d*) L. Aschwanden, T. Mallat, F. Krumeich and A. Baiker, *J. Mol. Catal. A*, 2009, **309**, 57; (*e*) B. L. Zhu, M. Lazar, B. G. Trewyn and R. J. Angelici, *J. Catal.*, 2008, **260**, 1; (*f*) J. P. Ma, Z. T. Du, J. Xu, Q. H. Chu and Y. Pang, *ChemSusChem*, 2011, **4**, 51; (*g*) T. Ishida, R. Takamura, T. Takei, T. Akita and M. Haruta, *Appl. Catal., A*, 2012, **413**, 261.
7 A. Abad, P. Concepcion, A. Corma and H. Garcia, *Angew. Chem., Int. Ed.*, 2005, **44**, 4066.
8 A. Tanaka, K. Hashimoto and H. Kominami, *J. Am. Chem. Soc.*, 2012, **134**, 14526.
9 (*a*) M. Alhumaimess, Z. J. Lin, W. H. Weng, N. Dimitratos, N. F. Dummer, S. H. Taylor, J. K. Bartley, C. J. Kiely and G. J. Hutchings, *ChemSusChem*, 2012, **5**, 125; (*b*) S. Mandal, K. K. Bando, C. Santra, S. Maity, O. O. James, D. Mehta and B. Chowdhury, *Appl. Catal., A*, 2013, **452**, 94; (*c*) M. J. Beier, T. W. Hansen and J. D. Grunwaldt, *J. Catal.*, 2009, **266**, 320.
10 L. Aschwanden, B. Panella, P. Rossbach, B. Keller and A. Baiker, *ChemCatChem*, 2009, **1**, 111.
11 L. Aschwanden, T. Mallat, M. Maciejewski, F. Krumeich and A. Baiker, *ChemCatChem*, 2010, **2**, 666.
12 H. X. Mai, L. D. Sun, Y. W. Zhang, R. Si, W. Feng, H. P. Zhang, H. C. Liu and C. H. Yan, *J. Phys. Chem. B*, 2005, **109**, 24380.
13 Z. L. Wu, M. J. Li, J. Howe, H. M. Meyer and S. H. Overbury, *Langmuir*, 2010, **26**, 16595.
14 M. Guo, J. Q. Lu, Y. N. Wu, Y. J. Wang and M. F. Luo, *Langmuir*, 2011, **27**, 3872.
15 T. X. T. Sayle, S. C. Parker and D. C. Sayle, *Phys. Chem. Chem. Phys.*, 2005, **7**, 2936.
16 M. Nolan, S. Grigoleit, D. C. Sayle, S. C. Parker and G. W. Watson, *Surf. Sci.*, 2005, **576**, 217.
17 (*a*) F. Wang, W. Ueda and J. Xu, *Angew. Chem., Int. Ed.*, 2012, **51**, 3883; (*b*) A. Abad, A. Corma and H. Garcia, *Chem.–Eur. J.*, 2008, **14**, 212.
18 M. K. Dalal, M. J. Upadhyay and R. N. Ram, *J. Mol. Catal. A*, 1999, **142**, 325.
19 F. Wang and W. Ueda, *Appl. Catal., A*, 2008, **346**, 155.
20 D. I. Enache, J. K. Edwards, P. Landon, B. Solsona-Espriu, A. F. Carley, A. A. Herzing, M. Watanabe, C. J. Kiely, D. W. Knight and G. J. Hutchings, *Science*, 2006, **311**, 362.
21 The TOF value is calculated based on the cationic gold.

